Active site electronic structure and dynamics during metalloenzyme catalysis

Oded Kleifeld[1], Anatoly Frenkel[2], Jan M.L. Martin[3] and Irit Sagi[1]

Published online 13 January 2003; doi:10.1038/nsb889

Zinc-dependent enzymes play important roles in many cellular processes. Assignment of their reaction mechanisms is often a subject of debate because the zinc ion is silent in several spectroscopic techniques. We have combined time-resolved X-ray absorption spectroscopy, pre-steady state kinetics and computational quantum chemistry to study the active site zinc ion of bacterial alcohol dehydrogenase during single substrate turnover. We detect a series of alternations in the coordination number and structure of the catalytic zinc ion with concomitant changes in metal–ligand bond distances. These structural changes are reflected in the effective charge of the metal ion. The present work emphasizes the flexibility of catalytic zinc sites during catalysis and provides novel mechanistic insights into alcohol dehydrogenase catalysis.

The study of catalytic active metal sites, especially those of zinc-dependent enzymes, is undergoing a renaissance because of the important roles these sites play in biological systems[1]. Understanding the molecular basis of events that drive catalysis in these systems is essential for the elucidation of the reaction mechanism. Classical enzymology and structural biology have provided insights into the reaction mechanisms of many metalloenzymes[2]. However, little structural information is available on intermediate states that evolve during catalysis of zinc-dependent enzymes, primarily because the zinc ion is silent for several spectroscopic techniques, including EPR and optical spectroscopy.

Here we examine the structural and electronic changes that occur at the catalytic site of a zinc metalloenzyme during substrate turnover by means of time-resolved X-ray absorption fine structure (XAFS) spectroscopy, pre-steady state kinetics and density functional theory (DFT) calculations. Using alcohol dehydrogenase from the thermophilic bacterium *Thermoanaerobacter brockii* (TbADH) as a representative zinc metalloenzyme (Fig. 1), we applied these experimental procedures to study the evolution of catalytic intermediate states during turnover. This tetrameric bacterial alcohol dehydrogenase (ADH) catalyzes the oxidation of secondary alcohols to their corresponding ketones with $NADP^+$ as the cofactor:

$$RCH(OH)R' + NADP^+ \leftrightarrow RC(O)R' + NADPH + H^+ \qquad (1)$$

The enzymatic reaction occurs through a compulsory ordered, ternary complex mechanism[3,4] and shows no subunit cooperativity. Both TbADH and the homologous ADH from *Clostridium beijerinckii* have been characterized by protein crystallography[5], and their reaction mechanism has been investigated by spectroscopic and kinetic studies[6]. Although inconclusive, the catalytic mechanism of TbADH was suggested to possibly be different than the one assigned to the horse liver ADH (HLADH)[5]. Nonetheless, as for other well-studied ADHs, the details of the reaction mechanism of these enzymes remain conjectural. Specifically, the intermediate states that evolve at the zinc ion during catalysis are still the subject of debate[7–10].

Several catalytic mechanisms for ADHs have been proposed on the basis of accumulating structural and spectroscopic evidence gathered from the most studied enzyme, HLADH[1,11]. The oxidation of alcohols requires a net removal of two hydrogen atoms from the substrate. This dehydrogenation process proceeds by coupled processes of proton abstraction and hydride ion transfer. The two main classes of structural mechanisms based on a proton relay system that have been proposed for HLADH differ specifically in the proposed coordination of the zinc ion during catalysis. One mechanism involves the displacement of the zinc-bound water by the alcohol substrate; therefore, the zinc ion remains tetrahedrally coordinated during catalysis[8,12]. In the alternative mechanism, the substrate molecule is added to the tetrahedral zinc ion to form pentacoordinated zinc[7,9]. These differences arise because there has been no direct time-dependent structural study so far to probe the catalytic zinc ion site during catalysis in such enzymatic systems.

As reported[13–18], probing metalloenzyme reactions by *in situ* X-ray absorption spectroscopy (XAS) is promising for explaining the changes that occur in critical metal centers during the course of the enzymatic reaction. Specifically for catalytic zinc sites, XAS is the only spectroscopic method that can provide high-resolution structural and electronic information in solution. We have used time-resolved XAS to determine the intermediate states at the first coordination shell of the catalytic zinc ion in TbADH during substrate turnover.

Trapping catalytic intermediates during single turnover

To trap catalytic intermediates at the zinc ion, we developed quantitative, time-dependent freeze-quench XAS procedures to follow the enzymatic reaction of TbADH under single turnover conditions. Following the formation of enzyme–substrate complexes during the first catalytic cycle improves the chances of synchronizing the evolving intermediate states that result from their relatively high concentrations within this time frame[19]. Lowering the reaction temperature resulted in slowing of the enzymatic rate of TbADH to the millisecond time scale. The pre-steady state kinetic profile of TbADH and 2-propanol, with

[1]Department of Structural Biology, The Weizmann Institute of Science, Rehovot 76100, Israel. [2]Department of Physics, Yeshiva University, New York, New York, 10016, USA. [3]Department of Organic Chemistry, Weizmann Institute of Science, Rehovot 76100, Israel.

Correspondence should be addressed to I.S. *e-mail: irit.sagi@weizmann.ac.il*

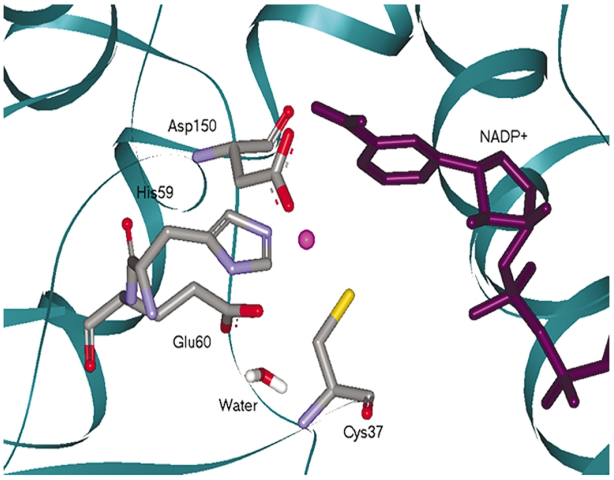

Fig. 1 The catalytic site in the TbADH–NADP+ complex (PDB entry 1YKF). The zinc ion (magenta) is bound to Cys37, His59, Asp150 and Glu60. The first coordination shell in TbADH is different than in most ADHs.

NADP+ as the leading substrate, was determined under stopped-flow conditions after the reduction of NADP+ at 340 nm. In these experiments, the enzyme was incubated with saturating amounts of NADP+ before mixing with the alcohol substrate. A progress curve of the first catalytic cycle at 10 °C (Fig. 2*a*) shows that after a lag period of 25 ms, quantitative reduction of NADP+ is seen as a burst from 25 to 60 ms, followed by a subsequent linear steady state phase starting at 70 ms.

Time-dependent freeze-quenched XAS samples were prepared, within the time frame of a single catalytic turnover of TbADH, by rapidly mixing the TbADH–NADP+ complex with 2-propanol in a stopped-flow apparatus equipped with a freeze-quench device. The X-ray absorption coefficient data of various time-dependent complexes were collected at the zinc K-edge. From the spectral variations in the time-dependent zinc K fluorescence intensity detected between 0 and 120 ms (Fig. 2*b*), distinct changes in spectral features can be observed during the first catalytic cycle (0–60 ms). These changes are more apparent in the radial distribution of the raw extended X-ray absorption fine structure (EXAFS) data, as presented by the Fourier transform (FT) spectra of the various time domains (Fig. 2*c*). The shape and amplitude of the first FT peak are directly related to the details of the atomic distribution of the protein residues within the first coordination shell. The variations in the first FT peak profile lie outside the noise level, indicating that the local structure around the catalytic zinc ion undergoes distinctive dynamic structural changes during turnover.

To quantitatively derive the local structure around the catalytic zinc ion to (i) obtain the number of different species in the samples at all time steps, (ii) identify the species and (iii) obtain

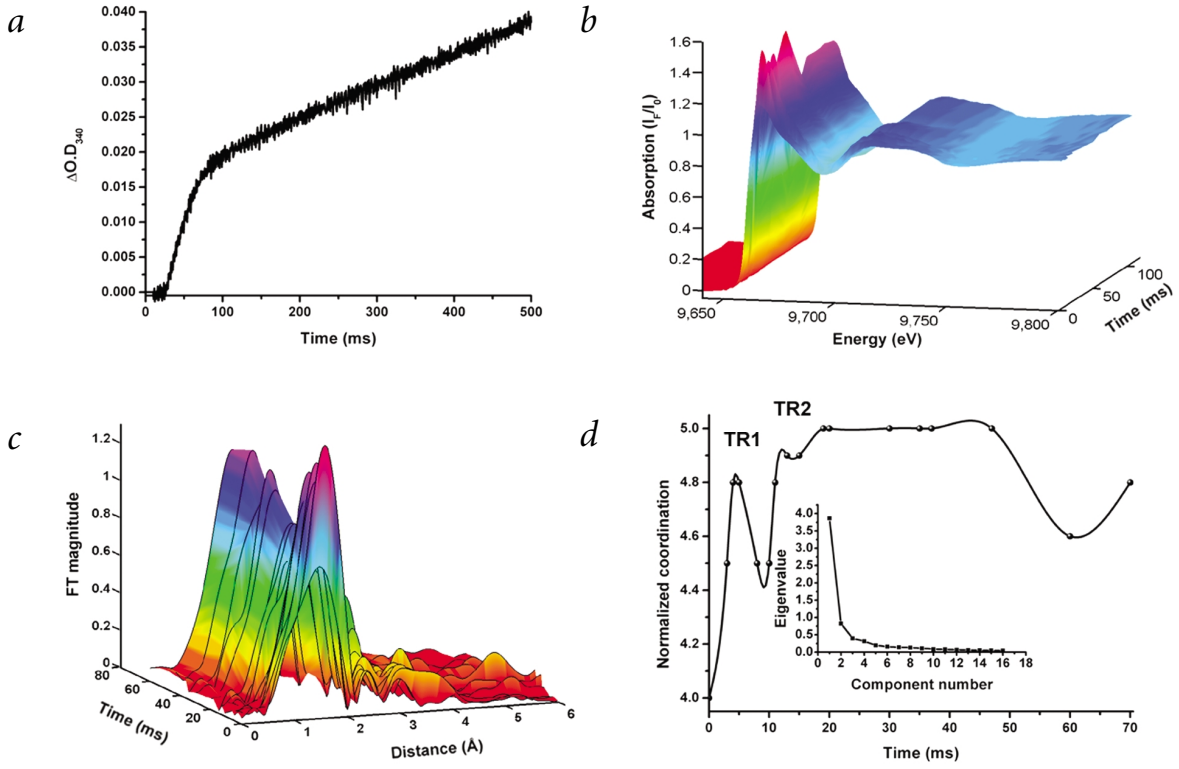

Fig. 2 Time-resolved freeze-quenched XAS of TbADH during a single catalytic cycle. ***a***, Determination of the time frame for a single catalytic cycle of TbADH reaction by pre-steady state kinetics. The quantitative reduction of NADP+ to NADPH occurs after a kinetic lag of 25 ms, followed by a burst between 25 and 60 ms and a subsequent linear steady state phase starting at 70 ms (at 10 °C). TbADH activity was monitored following the absorption increase at 340 nm (ε340 = 6.2 mM^{-1} cm^{-1}) for the formation of NADPH from NADP+. ***b***, Time-resolved freeze-quenched raw X-ray fluorescence data. Spectral changes can be observed within the time frame of single catalytic cycle (0–60 ms). ***c***, Magnitudes of the Fourier transform (FT) of k^2-weighted spectra, uncorrected for the photoelectron phase shifts, of the various time domains representing changes in the radial distribution of the zinc–ligand first shell environment during catalysis. ***d***, The change in coordination number during catalysis of TbADH. The coordination of the zinc ion expands from its original tetrahedral structure to the pentacoordinate complex by the addition of Zn-N/O contribution. Two distinct pentacoordinate intermediates, TR1 and TR2, evolve during the time frame of the kinetic lag phase. The normalized total coordination number is calculated by the relative fractions obtained from the RPA EXAFS analysis for each time point[20]. Insert, the PCA 'scree test' results demonstrating that all the time-dependent EXAFS spectra can be reproduced using two principal components.

Table1 XAS analysis of zinc–ligand intermediates during a single catalytic cycle of TbADH[1]

			Zn···N/O-I		Zn···N/O-II		Zn···S	
Time (ms)	Residual[2]	ΔE_0 (eV)[3]	R (Å)[4]	σ^2 (Å^2)[5]	R (Å)	σ^2 (Å^2)	R (Å)	σ^2 (Å^2)
0	100	1.0 (F)[6]	1×1.88 (1)	5.0×10^{-3}	2×2.00 (1)	4.0×10^{-3}	1×2.24 (1)	3.7×10^{-3}
3	60	–3.3 (F)	2×1.92 (1)	1.8×10^{-3}	2×2.14 (1)	1.2×10^{-3}	1×2.29 (F)	3.2×10^{-3}
4	80	–0.5 (F)	1×1.87 (2)	5.2×10^{-3}	3×1.99 (1)	1.0×10^{-6}	1×2.35 (F)	7.0×10^{-3}
5	80	–1.0 (F)	4×1.93 (1)	7.8×10^{-3}			1×2.25 (1)	6.3×10^{-4}
8	50	2.2 (F)	2×1.89 (2)	4.6×10^{-4}	2×2.02 (1)	2.6×10^{-4}	1×2.24 (2)	2.8×10^{-3}
10	50	–0.3 (F)	4×1.99 (1)	3.4×10^{-3}			1×2.37 (1)	4.0×10^{-3}
11	80	1.6 (F)	4×1.95 (1)	7.4×10^{-4}			1×2.27 (1)	1.0×10^{-5}
13	90	–1.7 (F)	2×1.85 (2)	1.8×10^{-3}	2×2.02 (1)	1.7×10^{-3}	1×2.25 (F)	1.0×10^{-6}
15	100	–1.9 (F)	1×1.79 (2)	1.0×10^{-6}	3×1.97 (1)	2.3×10^{-4}	1×2.33 (1)	6.8×10^{-3}
19	100	0.3 (F)	2×1.90 (1)	6.4×10^{-4}	2×2.13 (3)	6.4×10^{-4}	1×2.27 (F)	1.0×10^{-6}
20	100	–3.9 (F)	1×1.85 (1)	1.0×10^{-6}	3×2.00 (1)	2.6×10^{-3}	1×2.33 (2)	2.7×10^{-3}
30	100	–3.3 (F)	1×1.81 (4)	1.2×10^{-3}	3×1.96 (2)	2.5×10^{-3}	1×2.30 (1)	1.3×10^{-3}
35	100	–1.6 (F)	2×1.91 (3)	1.8×10^{-3}	2×2.01 (2)	2.2×10^{-3}	1×2.28 (F)	3.6×10^{-3}
37	100	2.6 (F)	4×2.00 (1)	7.3×10^{-3}			1×2.29 (F)	3.6×10^{-3}
47	100	–2.0 (F)	2×1.87 (1)	4.6×10^{-5}	2×2.02 (1)	4.0×10^{-3}	1×2.27 (1)	7.3×10^{-3}
60	60	–0.5 (F)	2×1.91 (1)	1.0×10^{-6}	2×2.07 (2)	1.4×10^{-3}	1×2.26 (F)	5.9×10^{-5}
70	80	–2.2 (F)	4×1.95 (1)	6.6×10^{-3}			1×2.28 (1)	1.0×10^{-6}

[1]Detailed fits are shown in *http://theochem.weizmann.ac.il/web/papers/trxas-nsb.html*. The starting complex (holo-TbADH) is represented in time 0, obtained by rapidly mixing and freeze-quenching the holo-TbADH with buffer prior to introducing the substrate. The rest of the fits are of the residual spectra resulting from iterative subtractions of fractions of the starting phases (time 0). Distinct expansion of ~0.15 ± 0.02 Å of two Zn···N/O bond distances is observed during the formation of the pentacoordinate intermediates TR1 at 3 ms and TR2 at 19 ms.
[2]Residual is designated as the residual fraction of the analyzed spectra.
[3]ΔE_0 is the correction to the energy origin.
[4]R is the distance from the zinc ion in Å. The uncertainties on the R parameter are shown in parentheses.
[5]σ^2 is the Debye-Waller factor.
[6]F indicates that the respective parameter was 'fixed' in the fit. Specific parameters were fixed after determining their best values by varying them in the fit using different initial conditions.

their mixing fractions within the various trapped complexes, we applied a novel combination of principal component analysis (PCA), multiple data-set fits (MDS) and residual phase analysis (RPA)[20] (data not shown, see *http://theochem.weizmann.ac.il/web/papers/trxas-nsb.html*). Using the PCA analysis, we show that two significant components are present at different fractional levels in all EXAFS spectra for each time step during initial substrate turnover (Fig. 2*d*, insert). The coordination number, metal–ligand bond distances and the Debye-Waller factors of each time-dependent spectrum were refined by iteratively subtracting different fractions (0–60%) of the known EXAFS spectrum of TbADH–$NADP^+$ complex — that is, the starting phase — and fitting the residual spectrum to theoretical amplitudes and phases calculated by means of FEFF 7 (ref. 21).

The coordination number of the catalytic zinc ion in TbADH changes dynamically during substrate turnover (Fig. 2*d*). The original tetrahedral coordination of the metal ion in the $NADP^+$ bound enzyme converts to a pentacoordinate structure by the addition of a scattering contribution from an oxygen or nitrogen atom in the inner coordination sphere. Specifically, two distinct pentacoordinate intermediate states, designated TR1 and TR2, were detected at 3–5 ms and 15–19 ms after mixing, respectively. The local structures around the catalytic zinc ion in these intermediates are consistent with first shell coordination of the zinc ion with four nitrogen or four oxygen atoms and one sulfur atom. In addition, distinct expansion of two Zn···N/O bond distances of ~0.15 ± 0.02 Å, relative to the starting zinc–ligand complex, is observed at these time points (Table 1). These pentacoordinate complexes were formed during the pre-steady state catalytic lag phase (during the first 25 ms) (Fig. 2*a*). In general, a kinetic lag phase detected during enzyme catalysis may be associated with conformational changes of the protein structure[22]. Our results show that the sequential evolution of the two pentacoordinate intermediate states reflects the structural reorganization of the catalytic zinc ion required for the subsequent hydride transfer process. Interestingly, similar analysis in the steady-state phase of the reaction shows that the decrease in coordination at the end of the first catalytic cycle is reversing (data not shown). However, the XAS data analysis is not conclusive for these time points, presumably because of the lack of synchronization between the evolving intermediate states and their relatively low concentrations within this time frame.

Such dynamic structural changes in coordination number and bond distances should be accompanied by changes in the electronic structure of the metal ion. To further examine this, we analyzed the change in the zinc K-edge energy upon interaction with the substrate. The absolute position of the edge energy contains information about the oxidation state of the absorbing atom[23]. Specifically, the shift to higher energy is associated with a more positive effective charge on the metal ion. Although zinc ions are generally not subject to drastic changes in oxidation states, we have reported previously that the formation of a pentacoordinate zinc complex upon inhibition of TbADH with dimethylsulfoxide (DMSO) resulted in the accumulation of partial positive charge on the metal ion[6]. The time-dependent change in edge position to higher energy is followed by a shift to lower energy during the course of TbADH catalysis (Fig. 3*a*). (These data were collected by time-resolved freeze-quench XAFS.)

Single-energy time-resolved XAS

To determine the profile of the change in edge energy during catalysis in real time, we conducted kinetic XAS experiments by measuring the X-ray fluorescence intensities at a single energy around the absorption edge using liquid stopped-flow cell. The change in the edge energy of the catalytic zinc ion of TbADH is directly correlated with the change in the effective charge of the

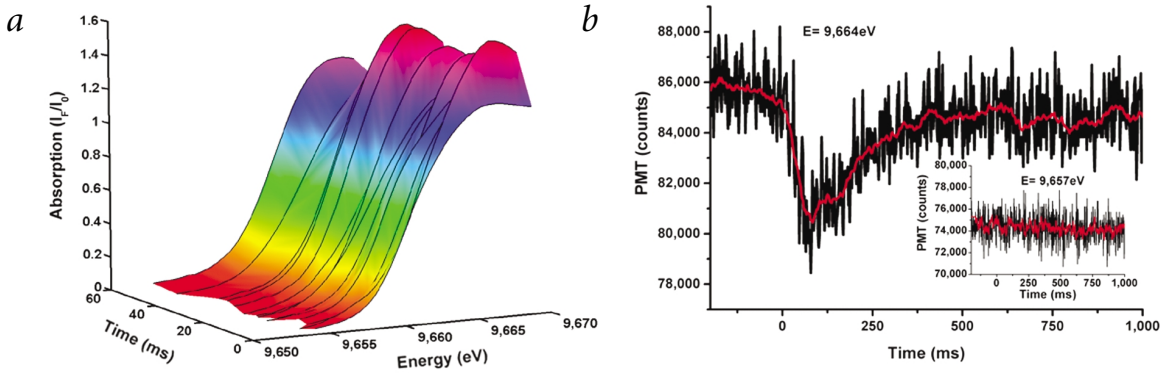

Fig. 3 Real-time changes in the effective charge of the catalytic zinc ion during TbADH catalysis. ***a***, The deviation in edge position during TbADH catalysis as detected by time-resolved freeze-quenched XAS. Shifts to higher energy are associated with accumulation of partial positive charge of the zinc ion. These changes are most pronounced at ~9,664 eV. ***b***, Single energy kinetic XAS results. The reduction in photon counts is correlated with the shift of the edge to higher energy and the accumulation of partial positive charge on the zinc ion. The detected dynamic profile of the edge shifts during TbADH catalysis, indicating a biphasic process composed of an initial rapid linear phase followed by a slow exponential phase. This dynamic profile is consistent with XAS and electronic structural calculations. Insert, the control experiment recorded below the edge at 9,657 eV shows no change in photon counts above the noise.

metal ion (Fig. 3*b*). We detected a distinct two-stage process, consisting of an initial rapid step followed by a slower 'exponential' step. Thus, the polarization of the catalytic zinc ion during substrate turnover, under the studied reaction conditions, is a sequential process, which is reflected in structural transitions within the coordination environment of the metal ion. Correlation with pre-steady state kinetics (Fig. 2*a*) indicates that the rapid change to higher energy occurs up to the middle of the burst. Thus, buildup of positive charge on the catalytic zinc ion can be correlated with the formation of the transient pentacoordinate intermediates (TR1 and TR2), whereas the hydride transfer process, product formation and release of product from the zinc ion 'neutralize' this effect. The change in the effective charge of the zinc ion in this 'neutralization' process is slower and shows a more complex profile than the initial reaction phase (Fig. 3*b*).

The accumulation of positive charge on the zinc ion can be explained by considering that the process of alcohol oxidation involves the following sequential steps (after $NADP^+$ binding): (i) alcohol binding, (ii) proton abstraction, (iii) hydride transfer and (iv) product release and cofactor release. In this respect, the process of proton abstraction may be related to the increase of partial positive charge on the metal ion. This requires that the proton abstraction occurs through the formation of a zinc-bound alcohol to alcoholate (R_2CHO^-), conversion and a transient metal-bound H_3O^+ species[9,24]. Formation of zinc bound alcoholate intermediate will withdraw electron density from the metal ion resulting in a more positive zinc ion.

Computational analysis

To explore the effect induced by the formation of a pentacoordinate structure on the effective charge of the zinc ion, we performed large basis set density functional theory calculations (details are provided in *http://theochem.weizmann.ac.il/web/papers/trxas-nsb.html*). The errors at the level of theory concerned are at least an order of magnitude smaller than the differences in properties discussed in this paragraph. The following three model systems were considered. System M1 consists of a Zn^{2+} atom with imidazole, methanethiol, acetate ion and water as ligands. System M2, in addition, has an isopropanol ligand *trans* to the water. In system M3, the isopropanol ligand was replaced by an acetone ligand. Partial charges on the Zn atom become more positive from the tetrahedral M1 to the trigonal bipyramid M2, using both the atomic polar tensor (APT)[25] definition (M1 = 1.453 and M2 = 1.574) and a natural population analysis (NPA)[26] (M1 = 1.566 and M2 = 1.593). This trend is consistent with the dynamic XAS data (Fig. 3). We note that the $Zn\cdots H_2O$ distance increases from 2.029 Å in M1 to 2.418 Å in M2, which is probably explained by the *trans* effect of the methanol ligand in M2. These results further suggest that the observed structural flexibility of the catalytic metal site is accompanied with distinct steps of the chemical reaction during enzymatic catalysis.

Reaction mechanism

The results reported here demonstrate the structural dynamics occurring at the catalytic zinc site during substrate turnover in the active site of the metalloenzyme. During a single catalytic cycle of the bacterial alcohol dehydrogenase TbADH, we detect two new pentacoordinate intermediate states, TR1 and TR2, which evolve at the zinc ion. The short lifetime of the first intermediate TR1 suggests that it functions as a precursor of TR2. Although the formation of TR2 results from the binding of the substrate, as can be assigned on the basis of pre-steady state kinetics (Fig. 2*a*) and inhibition results[6], the reproducible detection of TR1 was surprising. However, the formation of the TR1 intermediate with a pentacoordinate zinc ion is consistent with our recent observations of the dynamic role of the conserved zinc-bound Glu60 residue in TbADH. This residue is thought to be exchanged with a water molecule during catalysis of ADHs[27,28]. Specifically, we have replaced the Glu60 residue in TbADH by alanine. The steady state kinetic measurements show that the catalytic efficiency of this mutant is only two-fold lower than that of wild type TbADH (O.K., S. Shi, R. Zarivach, M. Eisenstein and I.S., unpub. data). Interestingly, XAS analysis of the variant enzyme in its native, cofactor-bound and inhibited forms (with DMSO) shows that the catalytic zinc site shows minor changes relative to the analogous complexes of wild type TbADH. These moderate changes in the kinetic parameters and in the first shell environment of the catalytic zinc ion imply that the Glu60 in TbADH does not remain bound to the metal ion during catalysis and may be exchanged by a water molecule. Such exchange may go through a pentacoordinate intermediate when both the water and the Glu60 residue are bound to the zinc ion before the dissociation of Glu60. On the basis of these

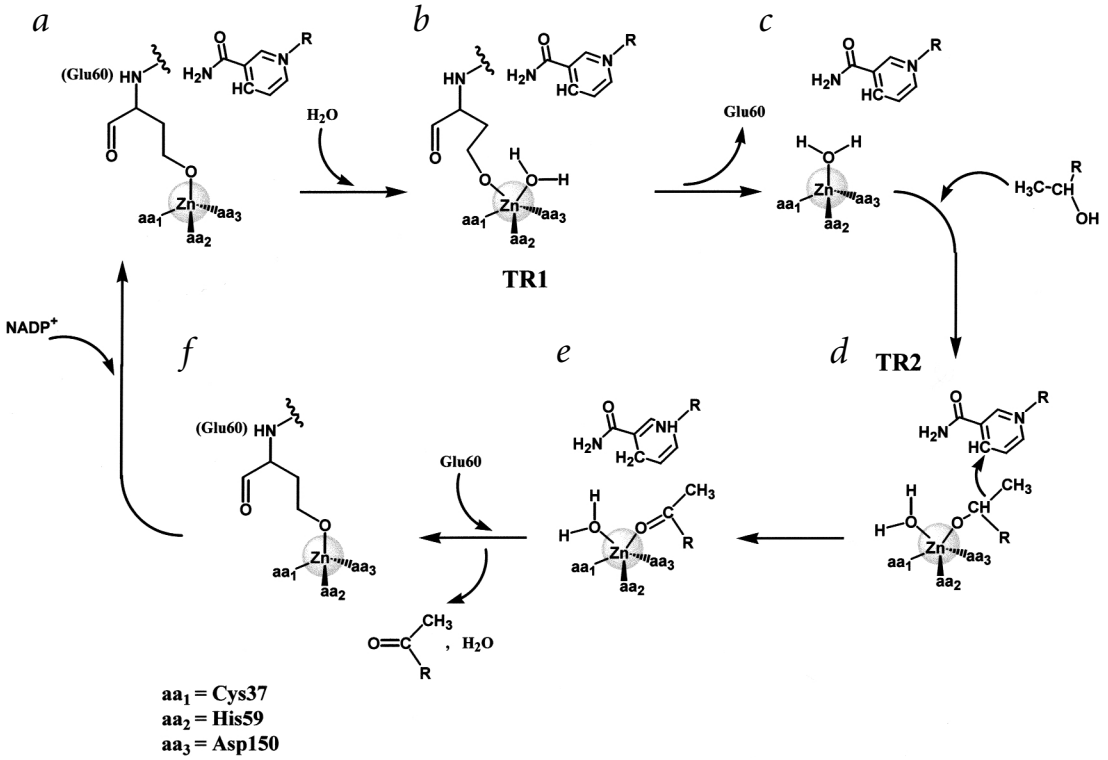

Fig. 4 Proposed structural events around the catalytic zinc ion in TbADH within the context of the reaction mechanism of the oxidation of secondary alcohols. **a**, The holoenzyme. The zinc ion remains tetrahedrally coordinated when bound to NADP+. In ***b***, the first transient complex (TR1) represents the coordination of a water molecule to the first coordination shell before the exchange of the Glu60 residue (see text). In ***c***, dissociation of the Glu60 residue results in a tetrahedral zinc ion with a bound water molecule. In ***d***, the binding of the alcohol substrate and the formation of alcoholate *via* hydride transfer produce the TR2 intermediate. ***e***, Formation of product. ***f***, Dissociation of the product, cofactor and water molecule and the subsequent binding of the Glu60 residue in the wild type conformation. The His59, Cys37 and Asp150 residues designated as aa1, aa2 and aa3, respectively, remain coordinated to the catalytic zinc ion during catalysis.

results, we propose a sequence of structural events occurring within the microenvironment of the catalytic zinc ion of TbADH during substrate turnover (Fig. 4). The coordination of the zinc ion in TbADH is dynamically altered from tetrahedral to pentacoordinate structure during catalysis. The formation of pentacoordinate intermediate during substrate turnover of TbADH is not in line with the proposed mechanism of a tetrahedrally coordinated zinc ion throughout ADH catalysis. However, the existence of such a transient intermediate may be supported by spectroscopic studies on cobalt-substituted HLADH[9,24] and, recently, the high-resolution crystal structures of HLADH[10]. Accordingly, our results further suggest that despite their different evolutionary origins, the reaction mechanism of HLADH and TbADH may possess common themes.

The application of quantitative time-resolved XAS to study catalytic zinc sites in enzymes reflects the unique properties of this metal in biological systems. Specifically, we identify electronic and structural flexibility at the nearest coordination shell of the zinc ion during catalysis. This novel structural dynamic information and the experimental approach may be used to study and refine reaction mechanisms in analogous systems.

Methods

Recombinant TbADH. Recombinant TbADH was produced and purified to homogeneity in a three-step purification scheme as described[29]. TG-1 cells transfected with TbADH-containing plasmid pBluescript II SK (+) (Stratgene) were grown for 16 h at 37 °C in 2YT medium with ampicillin (100 μg ml^{-1}). Pelleted cells were resuspended in 25 mM Tris-HCl, 0.1 mM dithiothreitol (DTT), 0.1 mM EDTA, 1 mM benzamidine and 0.02% sodium azide, pH 7.3 (buffer A). Cells were disrupted for 5 min by pulsed sonication (Branson Sonifier 450) on ice, followed by centrifugation at 23,000*g* for 15 min. The supernatant was heat treated for 10 min at 65 °C and then centrifuged again at 23,000*g* for 20 min. The supernatant was applied to a DEAE-sepharose column (Amersham Biosciences) (7 × 3 cm) at 4 °C and washed extensively with buffer A containing protease inhibitors. The recombinant protein was eluted from the column with a solution of 0.1 M NaCl in buffer A and applied to a Red Sepharose CL-6B column (Amersham Biosciences) (13 × 3 cm). The recombinant protein was eluted from the Red Sepharose column with a 400 ml NaCl linear gradient (0.1–1 M) in high yield (~300 mg l^{-1}) and with specific activity of 65–70 units mg^{-1} at 40 °C. The recombinant protein was dialyzed against 25 mM HEPES and 0.1 M NaCl, pH 8.3.

Pre-steady state kinetics. Transient kinetic experiments were carried out by using an Applied Photophysics SX.17MV stopped-flow apparatus with a thermostatic water circulating bath (measured dead time is 2 ms). TbADH activity was initiated by rapid mixing of 30 μM TbADH and 66 mM NADP+ with an equal volume of 200 mM 2-propanol. Both solutions were in buffer containing 25 mM HEPES and 100 mM NaCl. TbADH activity was monitored following the absorption increase at 340 nm wavelength (ε_{340} = 6.2 mM^{-1} cm^{-1}) for the formation of NADPH from NADP+.

Freeze-quenched sample preparation. The rapid-mix freeze-quenched samples were prepared using Bio-Logic SFM300 (measured dead time is 2 ms) equipped with freeze-quench apparatus for XAS[30]. The temperature of the system was controlled by a water bath (T = 10 °C). Equal volumes of 1 mM TbADH with 66 mM NADP+ and 200 mM 2-propanol were rapidly mixed and frozen. The zero

point sample was prepared by rapidly mixing the enzyme solution with buffer in the stopped flow apparatus following rapid freezing. Samples were stored in liquid nitrogen. Data were collected on frozen samples using four independent sample preparations made of different batches of enzyme and freshly prepared solutions. Lowering the reaction temperature of TbADH to 10 °C did not affect the integrity of the enzyme, as judged by SDS-PAGE and steady state kinetic assays.

XAS data collection. XAS data collection was performed at the National Synchrotron Light Source at Brookhaven National Laboratory, beamline X9B. The frozen samples were then mounted into a Displex closed-cycle He cryostat, and their temperatures were maintained at 30 K to minimize the thermal disorder in the XAS data. The incident beam intensity was recorded using an ionization chamber, and the fluorescence intensity was recorded using a 13-element Ge detector. The transmission signal from a zinc foil was measured with a reference ion chamber simultaneously with fluorescence for the purpose of beam energy calibration.

XAS data processing and analysis. The raw Zn K-edge absorption coefficient data, $\mu(E)$, were averaged over several consecutive XAS measurements for each sample and aligned in absolute energy using the reference Zn metal foil XAS data for calibration. The smooth atomic background was removed from all the $\mu(E)$ data using the AUTOBK program of the UWXAFS data analysis package[31], and the EXAFS $\chi(k)$ data, where k is the photoelectron wave number, were obtained. The structural model for fitting the experimental data was constructed using the crystallographic coordinates of holo-CbADH (PDB entry 1KEV). The theoretical photoelectron scattering amplitudes and phase shifts were calculated using FEFF 7 (refs 21,32). The theoretical EXAFS signal was fit to the experimental data using the non-linear least squares method implemented in FEFFIT 2.54 (ref. 31). The number of different species in the samples at all time steps and the mixing fractions within the various trapped complexes were determined by applying PCA, multiple data-set fits and residual phase analysis[20] (data not shown; see *http://theochem.weizmann.ac.il/web/papers/trxas-nsb.html*).

Single energy kinetic XAS experiments. Real-time kinetic XAS experiments were collected at 4 °C under the same reaction conditions used for the freeze-quench experiments. The reaction rate at this temperature was reduced by an additional factor of ~0.25 compared with the rate measured at 10 °C. These experiments were conducted at the Advance Photon Source (APS) at the Argonne National Laboratory, beamline Bio-CAT. Data were collected by synchronizing the shutters of a liquid stopped-flow device (dead time of 10 ms) with the X-ray source and with data acquisition (*http://www.bio.aps.anl.gov/biocat*). X-ray fluorescence data were recorded by a fast PMT tube and stored in millisecond bin arrays using the APEX system.

EXAFS data processing and analysis. Details of the data analysis are not shown; see *http://theochem.weizmann.ac.il/web/papers/trxas-nsb.html*.

Electronic structure calculations. All electronic structure calculations were carried out using the Gaussian 98 system[33]. For details see *http://theochem.weizmann.ac.il/web/papers/trxas-nsb-html/*.

Acknowledgments

We thank M. Sullivan from the NSLS beam line X9B, K. Zhang and S. Stepanov from the APS the BioCat beamline and G. Kafri and E. Yavin from the Weizmann Institute for their help and technical advice. The authors are grateful to M.W. Makinen for critically reading this manuscript. This work was supported by the Israeli Science Foundation (I.S.) and by the Minerva Foundation (J.M.L.M.).

Competing interests statement

The authors declare that they have no competing financial interests.

Received 11 September, 2002; accepted 3 December, 2002.

1. Auld, D.S. Zinc coordination sphere in biochemical zinc sites. *Biometals* **14**, 271–313 (2001).
2. Karlin, K.D. Metalloenzymes, structural motifs, and inorganic models. *Science* **261**, 701–708 (1993).
3. Oestreicher, E.G., Pereira, D.A. & Pinto, G.F. Steady-state kinetic mechanism of *Thermoanaerobacter brockii* alcohol dehydrogenase: a study discrimination between alternative kinetic models. *J. Biotechnol.* **46**, 23–31 (1996).
4. al-Kassim, L.S. & Tsai, C.S. Studies of $NADP^+$-preferred secondary alcohol dehydrogenase from *Thermoanaerobium brockii*. *Biochem. Cell Biol.* **68**, 907–913 (1990).
5. Korkhin, Y. *et al*. NADP-dependent bacterial alcohol dehydrogenases: crystal structure, cofactor-binding and cofactor specificity of the ADHs of *Clostridium beijerinckii* and *Thermoanaerobacter brockii*. *J. Mol. Biol.* **278**, 967–981 (1998).
6. Kleifeld, O. *et al*. Spectroscopic studies of inhibited alcohol dehydrogenase from *Thermoanaerobacter brockii*: proposed structure for the catalytic intermediate state. *Biochemistry* **39**, 7702–7711 (2000).
7. Dworschack, R.T. & Plapp, B.V. Kinetics of native and activated isozymes of horse liver alcohol dehydrogenase. *Biochemistry* **16**, 111–116 (1977).
8. Dunn, M.F., Biellmann, J.F. & Branlant, G. Roles of zinc ion and reduced coenzyme in horse liver alcohol dehydrogenase catalysis. The mechanism of aldehyde activation. *Biochemistry* **14**, 3176–3182 (1975).
9. Makinen, M.W., Maret, W. & Yim, M.B. Neutral metal-bound water is the base catalyst in liver alcohol dehydrogenase. *Proc. Natl. Acad. Sci. USA* **80**, 2584–2588 (1983).
10. Meijers, R. *et al*. On the enzymatic activation of NADH. *J. Biol. Chem.* **276**, 9316–9321 (2001).
11. Dunn, M.F., MacGibbon, A.K.H. & Pease, K. Liver alcohol dehydrogenase:electrostatic strain-distortion effects facilitate hydride ion transfer. in *Zinc Enzymes*, Vol. 1 (eds. Bertini, I., Luchinat, C., Maret, W. & Zeppezauer, M.) 378–534 (Birkhauser Boston, Boston; 1986).
12. Eklund, H., Plapp, B.V., Samama, J.P. & Branden, C.I. Binding of substrate in a ternary complex of horse liver alcohol dehydrogenase. *J. Biol. Chem.* **257**, 14349–14358 (1982).
13. Powers, L., Sessler, L., Woolery, G.L. & Chance, B. CO bond angle changes in photolysis of carboxymyoglobin. *Biochemistry* **23**, 5519–5523 (1984).
14. Scheuring, E.M. *et al*. Time-resolved X-ray absorption spectroscopy of photoreduced base-off Cob(II)alamin compared to the Co(II) species in *Clostridium thermoaceticum*. *J. Phys. Chem.* **100**, 3344–3348 (1996).
15. Chance, M.R. *et al*. Global mapping of structural solutions provided by the extended X-ray absorption fine structure *ab initio* code FEFF 6.01: structure of the cryogenic photoproduct of the myoglobin-carbon monoxide complex. *Biochemistry* **35**, 9014–9023 (1996).
16. Riggs-Gelasco, P. *et al*. EXAFS characterization of the intermediate X generated during the assembly of the *E. coli* ribonucleotide reductase R2 diferric tyrosyl radical cofactor. *J. Am. Chem. Soc.* **120**, 849–860 (1998).
17. Hwang, J. *et al*. A short Fe-Fe distance in peroxodiferric ferritin: control of Fe substrate *versus* cofactor decay? *Science* **287**, 122–125 (2000).
18. Lee, S.K. *et al*. Nature of the intermediate formed in the reduction of O_2 to H_2O at the trinuclear copper cluster active site in native laccase. *J. Am. Chem. Soc.* **124**, 6180–6193 (2002).
19. Fersht, A. The basic equations of enzyme kinetics. in *Structure and Mechanism in Protein Science* (eds. Julet, M.R. & Hadler, G.L.) 103–131 (W.H. Freeman, New York; 1999).
20. Frenkel, A., Kleifeld, O., Wasserman, S.R. & Sagi, I. Phase speciation by extended X-ray-absorption fine structure spectroscopy. *J. Chem. Phys.* **116**, 9449–9456 (2002).
21. Zabinsky, S.I., Rehr, J.J., Ankudinov A., Albers R.C. & Eller M.J. Multiple scattering calculations of X-ray absorption spectra. *Phys. Rev. B* **52**, 2995–3009 (1995).
22. Frieden, C. Slow transitions and hysteretic behavior in enzymes. *Ann. Rev. Biochem.* **48**, 471–489 (1979).
23. Bianconi, A. XANES spectroscopy. in *X-Ray Absorption*, Vol. 92 (eds. Koningsberger, D.C. & Prins, R.) 573–662 (John Wiley & Sons, New York; 1988).
24. Maret, W. & Makinen, M.W. The pH variation of steady-state kinetic parameters of site-specific Co^{2+}-reconstituted liver alcohol dehydrogenase a mechanistic probe for the assignment of metal-linked inoziations. *J. Biol. Chem.* **266**, 20636–20644 (1991).
25. Cioslowski, J. A new population analysis based on atomic polar tensors. *J. Am. Chem. Soc.* **111**, 8333–8336 (1989).
26. Reed, A.E., Curtiss, L.A. & Weinhold, F. Intermolecular interactions from a natural bond orbital, donor-acceptor viewpoint. *Chem. Rev.* **88**, 899–926 (1988).
27. Ryde, U. On the role of Glu68 in alcohol dehydrogenase. *Protein Sci.* **4**, 1124–1132 (1995).
28. Yang, Z.N., Bosron, W.F. & Hurley, T.D. Structure of human chi chi alcohol dehydrogenase: a glutathione-dependent formaldehyde dehydrogenase. *J. Mol. Biol.* **265**, 330–343 (1997).
29. Bogin, O., Peretz, M. & Burstein, Y. *Thermoanaerobacter brockii* alcohol dehydrogenase: characterization of the active site metal and its ligand amino acids. *Protein Sci.* **6**, 450–458 (1997).
30. Appleyard, R.J., Shuttleworth, W.A. & Evans, J.N. Time-resolved solid-state NMR spectroscopy of 5-enolpyruvylshikimate-3-phosphate synthase. *Biochemistry* **33**, 6812–6821 (1994).
31. Stern, E.A., Newville, M., Ravel, B., Yacoby, Y. & Haskel, D. The UWXAFS analysis package: philosophy and details. *Physica B* **208-209**, 117–120 (1995).
32. Rehr, J.J., Mustre de Leon, J., Zabinsky, S.I. & Albers, R.C. Theoretical X-ray absorption fine structure standards. *J. Am. Chem. Soc.* **113**, 5135–5140 (1991).
33. Frisch, M.J. *et al*. Gaussian 98. (Rev. A.11) (Gaussian, Inc., Pittsburgh; 2001).